Electronic Supplementary Information (ESI) for: Relating Structural Phase Transitions to Mechanoluminescence: The Case of the $Ca_{1-x}Sr_xAl_2Si_2O_8$:1%Eu^{2+},1%Pr^{3+} Anorthite

Ang Feng[a,b], Simon Michels[a,b], Alfredo Lamberti[c], Wim Van Paepegem[c], Philippe F. Smet[a,b,*]

[a] *LumiLab, Department of Solid State Sciences, Ghent University, Krijgslaan 281-S1, 9000 Gent, Belgium*
[b] *Center for Nano and Biophotonics (NB-Photonics), Ghent University, 9000 Gent, Belgium*
[c] *Mechanics of Materials and Structures (MMS), Department of Materials, Textiles and Chemical Engineering (MaTCh), Ghent University, Tech Lane Ghent Science Park 46, 9052 Zwijnaarde, Belgium*

Abstract

This is the electronic supplementary information (ESI) for the article entitled '**Relating Structural Phase Transitions to Mechanoluminescence: The Case of the $Ca_{1-x}Sr_xAl_2Si_2O_8$:1%Eu^{2+},1%Pr^{3+} Anorthite**'. It includes supplementary information on (1) the scanning electron microscopy (SEM) images of anorthites, (2) their cell parameters from Rietveld refinement, (3) methods of extracting electron population functions and (4) TL curves as a function of Delay time for $x_{Sr} = 0.00$ and 0.10.

1. Morphology of Anorthites

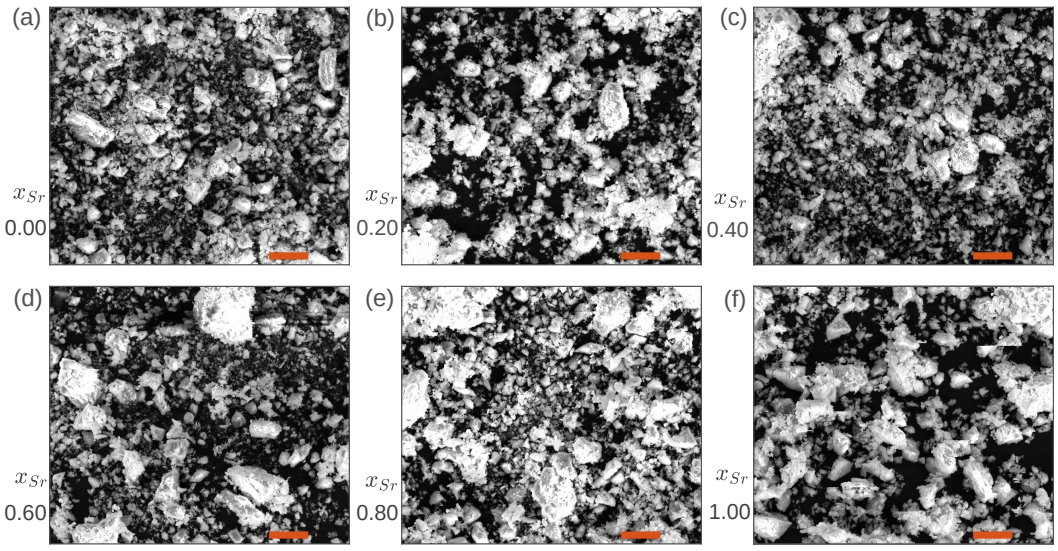

Figure S1: Typical SEM images of anorthites with different strontium (x_{Sr}), (a) 0.00, (b) 0.20, (c) 0.40, (d) 0.60, (e) 0.80, and (f) 1.00. The scale bar is 20 μm. (Quanta 200F (FEI) electron microscope, voltage 20 kV)

The solid-state reaction method leads to anorthites with the intended chemical composition. These phosphors are typically irregularly-shaped particles with diameters ranging from $\sim$ 1 μm to $\sim$ 30 μm, as

*Corresponding author
Email address: Philippe.Smet@UGent.be (Philippe F. Smet)

shown in Figure S1. The morphologies of these phosphors are consistent for different x_{Sr}, validating the comparison of their optical properties.

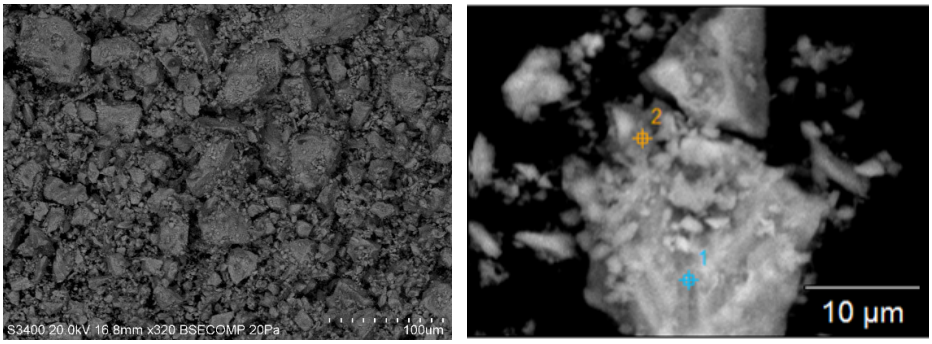

(a) (b)

Figure S2: Back scattered SEM image **(a)** shows that the $SrAl_2Si_2O_8$ powder is quite homogeneous and **(b)** a closer look reveals that a few Al-rich impurities (point 2) are present, evidenced by atomic ratio calculation by EDX (Table S1). (Hitachi S3400 electron microscope, voltage 20 kV)

There are tiny amounts of α-Al_2O_3 as impurities in these phosphors. For example, the Sr end-member is quite homogeneous (Figure S2a), with a small amount of Al-rich phases, which were assumed to be α-Al_2O_3. This was confirmed by energy dispersive X-ray (EDX) analysis of the positions chosen in Figure S2b, and the results were listed in Table S1.

Table S1: Atomic ratio with respect to Sr by EDX for two selected point in Figure S2b, revealing the presence of Al-rich phases.

Position	Al/Sr	Si/Sr	O/Sr	
1	1.57	2.12	5.46	
2	5.92	2.19	13.6	
-	2.0	2.0	8.0	theoretical

2. Structure of Anorthites

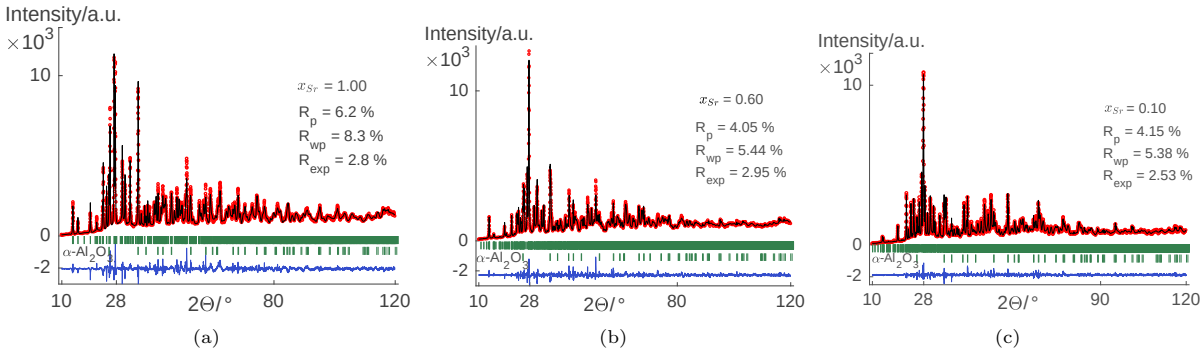

Figure S3: The Rietveld refinement profiles for **(a)** $x_{Sr} = 1.00$, **(b)** $x_{Sr} = 0.60$, and **(c)** $x_{Sr} = 0.10$. The α-Al_2O_3 was regarded as impurity, and small R values indicate a good refinement. (red: experimental XRD; black: calculated; blue: difference; green: reflection position.)

The Rietveld refinement was carried out by the Fullprof Suite [1]. The background for each refinement was manually selected because of the complexity of the XRD patterns. The B_{iso} for all atoms are set to

zero, and atomic occupation were the theoretical values from the chemical formula. Including α-Al_2O_3 as an impurity leads to better Rietveld refinement. For example, the calculated XRD pattern for the Sr end-member, $x_{Sr} = 0.60$ and 0.10 are shown in Figure S3a,S3b,S3c, respectively.

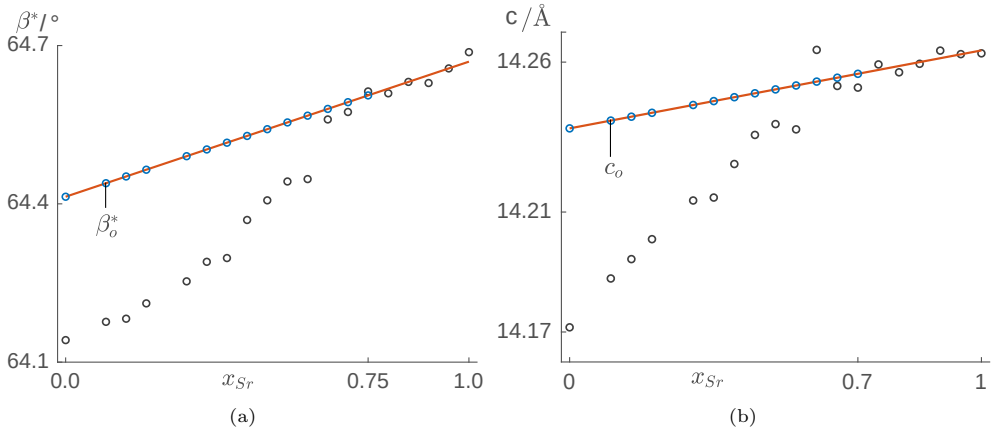

Figure S4: The β^*_o **(a)** and c_o **(b)** values (blue open circles) were extrapolated linearly from their corresponding values (grey open circles) in the $I\frac{2}{c}$ phases.

A linear extrapolation scheme was adopted to obtain c_o and β^*_o, as shown Figure S4a and S4b, respectively. Here, symbol o denotes the reference state in $I\bar{1}$ extrapolated from $I\frac{2}{c}$ as if the phase transition had not taken place, and the $*$ designates reciprocal space. Therefore, we have [2],

$$cos\beta^* = \frac{cos\gamma \cdot cos\alpha - cos\beta}{sin\gamma \cdot sin\alpha}. \tag{1}$$

The results were tabulated in Table S2.

Table S2: The cell parameters of $Ca_{1-x}Sr_xAl_2Si_2O_8$:1%Eu^{2+},1%Pr^{3+} from Rietveld refinement.

x_{Sr}	a/Å	b/Å	c/Å	α/°	β/°	γ/°	V/Å^3	β^*/°	β^*_o/°	c_o/Å
0.00	8.1846	12.8752	14.1716	93.1349	115.7376	91.2024	1341.536	64.1418	64.4135	14.2379
0.10	8.2103	12.8876	14.1878	92.9541	115.7135	91.1780	1349.237	64.1764	64.4391	14.2405
0.15	8.2212	12.8912	14.1943	92.8650	115.7132	91.1566	1352.207	64.1823	64.4519	14.2418
0.20	8.2362	12.8986	14.2010	92.7367	115.6933	91.1056	1356.583	64.2144	64.4647	14.2431
0.30	8.2611	12.9112	12.2139	92.4660	115.6635	91.1028	1364.083	64.2531	64.4903	14.2457
0.35	8.2709	12.9140	14.2148	92.3072	115.6347	91.0741	1366.635	64.2902	64.5031	14.2470
0.40	8.2856	12.9256	14.2260	92.1147	115.6382	91.0121	1371.662	64.2973	64.5159	14.2483
0.45	8.3046	129,354	14.2357	91.8272	115.5830	90.9321	1377.119	64.3694	64.5287	14.2496
0.50	8.3136	12.9354	14.2393	91.6537	115.5487	90.9273	1380.621	64.4067	64.5415	14.2509
0.55	8.3186	12.9419	14.2378	91.4961	115.5189	90.8956	1382.199	64.4424	64.5543	14.2522
0.60	8.3363	12.9671	14.2571	91.3170	115.5210	90.8546	1389.893	64.4469	64.5671	14.2535
0.65	8.3481	12.9680	14.2521	90.5999	115.4329	90.4164	1393.174	64.5600	64.5799	14.2548
0.70	8.3530	12.9677	14.2515	90.4475	115.4222	90.3084	1394.118	64.5741	64.5927	14.2561
0.75	8.3656	12.9736	14.5923	90	115.3870	90	1398.129	64.6130	64.6130	14.2592
0.80	8.3663	12.9720	14.2566	90	115.3905	90	1397.788	64.6095	64.6095	14.2566
0.85	8.3727	12.9712	14.2594	90	115.3689	90	1399.492	64.6311	64.6311	14.2594
0.90	8.3789	12.9756	14.2638	90	115.3710	90	1401.203	64.6290	64.6290	14.2638
0.95	8.3794	12.9727	14.2617	90	115.3432	90	1401.198	64.6567	64.6567	14.2627
1.00	8.3857	12.9743	14.2629	90	115.3125	90	1402.371	64.6875	64.6875	14.2629

3. Electron Population Function

The electron population function $n(E_{trap}, t)$ was extracted from the T_m-T_{stop} method [3]. The electron population function is the product of the trap distribution $N(E_{trap})$ and the filling function $f(t, E_{trap}, q)$. In the trap depth interval $(E_{trap}, E_{trap} + dE)$, the number of electrons is,

$$dn(E_{trap}, t) = N(E_{trap}) f(E_{trap}, t, q) dE. \tag{2}$$

The T_m-T_{stop} method requires that the phosphors be charged at a fixed temperature and then partially cleaned, emptying certain traps by rising the temperature to T_{stop} [3].

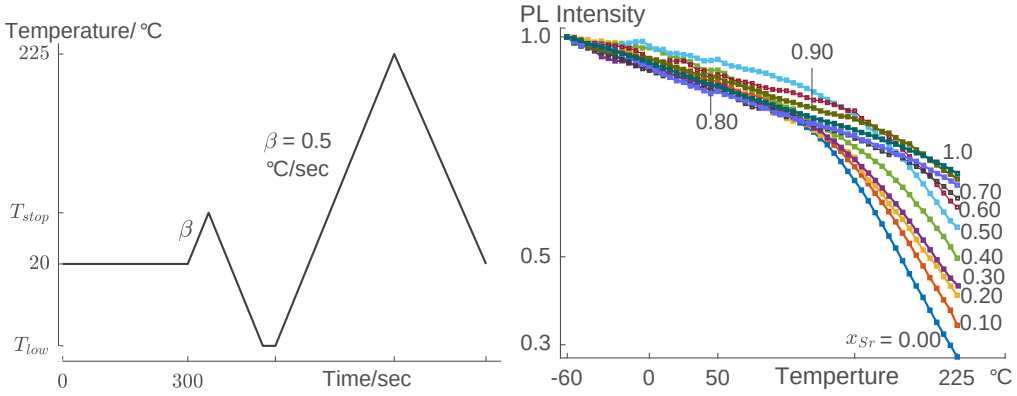

Figure S5: The schematic drawing **(a)** of the procedure for T_m-T_{stop} method, and **(b)** the thermal quenching profiles used to correct the TL profiles.

A typical heating procedure was shown in Figure S5a, and the temperature T_{low} was chosen in order to have a minimal or negligible afterglow intensity. All TL profiles have been corrected by the thermal quenching function (Figure S5b). Therefore, the very shallow and very deep traps cannot be filled by charging, due to the improper charging temperature, thermal detrapping, or optically stimulated detrapping. In such a T_m-T_{stop} method, the area between neighboring TL curves was estimated as the electron population in the trap depth interval corresponding to the TL curves.

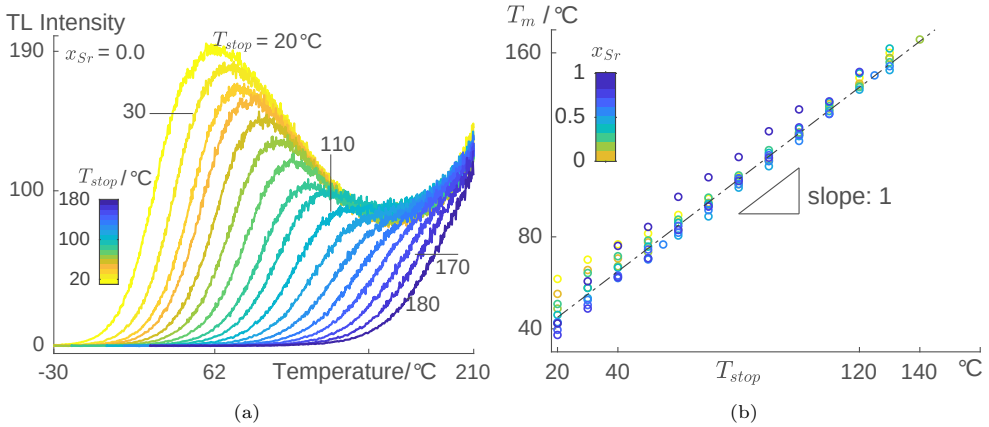

Figure S6: TL curves **(a)** for T_{stop} ranging from 20-180 °C for $Ca_{1-x}Sr_xAl_2Si_2O_8$:1%Eu^{2+},1%Pr^{3+} ($x_{Sr} = 0.00$), and **(b)** a linear relationship was found between T_m and T_{stop} for all x_{Sr}, with a slope roughly equal to 1.0.

The TL peak maxima decrease with increasing T_{stop}, which means more detrapping of electrons from traps (Figure S6a). A distribution of trap depths will normally shift the temperature corresponding to the TL peak maxima, T_m. A linear relationship between T_m and T_{stop} indicates a continuous distribution of traps (Figure S6b) [3]. Generally, a perfectly equal energy interval extracted from the T_m data is not always possible. Here, we use a linear interpolation to map the data group $(T_m, totalTL)$ into a uniform grid of E_{trap} using the Urbach relation [4] $E_{trap} = T_m/500$. A plot of E_{trap} against the difference in $totalTL$ will result in the electron population function, as shown in Figure S7. Note, in the main text, the electron population function was converted to its probability density function (excluding deep traps) by proper normalization. It is worthy to note that the electron population function depends on time t. The method adopted here does not include a delay between charging and heating to T_{stop}, and it results in an electron population function around Delay time $\simeq 0$ sec.

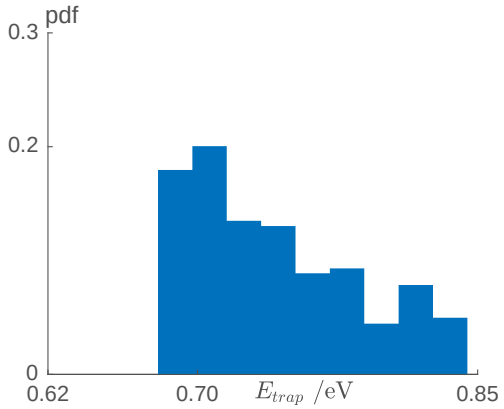

Figure S7: The probability density function (pdf) of electron population $n\,(E_{trap}, t)$ for $x_{Sr} = 0.00$ when $t \simeq 0$, which gives a broad distribution for shallow-intermediate traps (< 0.85 eV).

4. TL Profile as a Function of Delay for $x_{Sr} = 0.00$ and 0.10

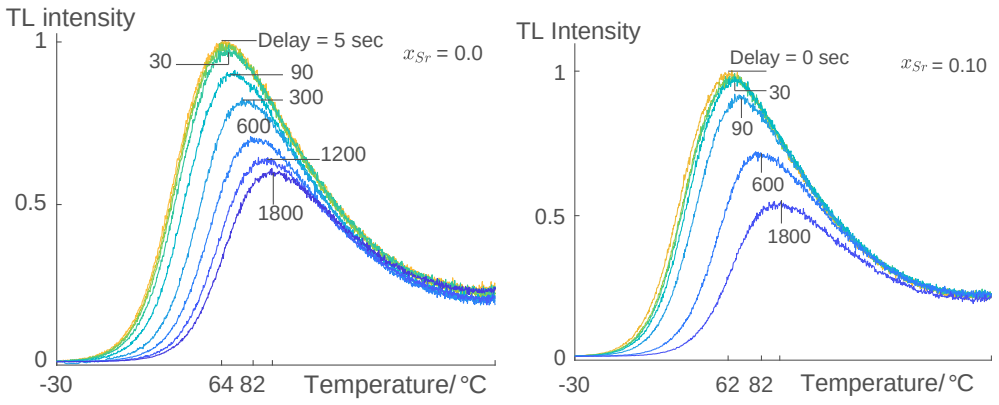

(a) (b)

Figure S8: The TL intensities as a function of Delay time for **(a)** $x_{Sr} = 0.00$,and for **(b)** $x_{Sr} = 0.10$.

The electron population function will change with Delay, but a prominent change is only expected in the shallow traps, since deep traps are not thermally accessible easily at room temperature. The TL intensities as a function of Delay timefor $x_{Sr} = 0.00$ (Figure S8a) and $x_{Sr} = 0.10$ (Figure S8b) show a shift of T_m up

to $\sim$ 20 K when the Delay reaches around 600 sec, which corresponds to a shift of $\sim$ 0.04 eV in trap depth. A shift of $\sim$ 30 K in T_m can be obtained when the Delay time reaches around 1800 sec, when the actual AG is quite low and ML signals are usually not detectable above the background noise.

References

[1] J. Rodríguez-Carvajal, Recent advances in magnetic structure determination by neutron powder diffraction, Physica B 192 (1) (1993) 55–69. doi:10.1016/0921-4526(93)90108-I.

[2] U. Shmueli, Reciprocal space in crystallography, Springer Netherlands, Dordrecht, 2001, pp. 2–9. doi:10.1107/97809553602060000549.

[3] S. W. S. McKeever, On the analysis of complex thermoluminescence glow-curves: Resolution into individual peaks, Phys. Status Solidi A 62 (1) (1980) 331–340. doi:10.1002/pssa.2210620139.

[4] F. Urbach, Zur lumineszenz der alkalihalogenide, Sitzungsberichte Akad. der Wiss. Wien 139 (1930) 363–372.